promotes the mobility of oxygen and Vö in the TiO_2 oxide lattice. The movement of oxygen and Vö can produce a gradient of charges in polarized MAO TiO_2. Although the surface OH groups on the Ti surface and the removal of adsorbed organic contaminants are assumed to play important roles in photoinduced hydrophilicity [40,41], other factors such as hydration forces have also recently been studied [42,43]. In this study the wettability of the polarized samples was not correlated with the number of surface OH and absorbed organic species. One factor that produced a lasting reduction in the water contact angle might be the electrowetting effect. The electrowetting effect can be defined as a change in the solid–liquid contact angle due to an electric field applied to the solid and the liquid [44]. The forces that result from the applied electric field tend to pull the droplet down onto the electrode, lowering the macroscopic contact angle and increasing the droplet contact area [45]. The electric polarization treatment in this experiment resulted in the formation of a capacitor at the interface between the TiO_2 surfaces and deionized water, partially dissociated into H_3O^+ and OH^- at room temperature. The electrostatic forces decrease the surface energy and the contact angle. Because there were equal quantities of stored electric charges on the N surface and the P surface the enduring reduction in contact angle was nearly the same on both surfaces [19,20]. Similar results have also been observed in other research where both positive and negative surfaces showed symmetrical electrowetting [46,47].

4. Conclusions

The experimental results demonstrated that MAO TiO_2 coatings are polarizable materials, similar to previous reports regarding other bioceramics. The metastable state produced by the electric fields induced surface charges on both surfaces, termed the N surface and the P surface. The polarized MAO TiO_2 surfaces do not exhibit any obvious changes in morphology, surface roughness or phase components in SEM, EDX and XRD observations. However, the electric polarization treatment resulted in changes to the surface chemical composition and the surface wettability. XPS analysis revealed that the oxygen binding energies of the three surfaces were different, and several days after the procedure the polarized surfaces became more hydrophilic than the non-polarized surface due to the induced surface charges. The polarized MAO TiO_2 has good geometry and lasting wettability, suggesting potential uses in the surface modification of Ti implants.

Acknowledgements

This work was supported by the Nippon Foundation–Sasakawa Memorial Health Foundation Program, Japan, and Grants-in-Aid for Scientific Research (C) (20500405) from the Japan Society for the Promotion of Science.

Appendix A. Figures with essential colour discrimination

Certain figures in this article, particularly Figure 2, are difficult to interpret in black and white. The full colour images can be found in the on-line version, at doi:10.1016/j.actbio.2011.09.021.

References

[1] Brunette DM, Tengvall P, Textor M, Thomsen P. Titanium in medicine: material science, surface science, engineering, biological response and medical applications. Berlin: Springer Verlag; 2001.
[2] Long M, Rack HJ. Titanium alloy in total joint replacement – a materials science perspective. Biomaterials 1998;19:1621–39.
[3] Li J, Hastings GW. Oxide ceramics: inert ceramic materials in medicine and dentistry. In: Black J, Hastings G, editors. Handbook of biomaterial properties. London: Chapman & Hall; 1998. p. 340–54.
[4] Liu XY, Paul KC, Ding CX. Surface modification of titanium, titanium alloys, and related materials for biomedical applications. Mater Sci Eng R 2004;47:49–121.
[5] Junker R, Dimakis A, Thoneick M, Jansen JA. Effects of implant surface coatings and composition on bone integration: a systematic review. Clin Oral Implants Res 2009;20:185–206.
[6] Ishizawa H, Ogino M. Formation and characterization of anodic titanium oxide films containing Ca and P. J Biomed Mater Res 1995;29:65–72.
[7] Yerokhin AL, Nie X, Leyland A, Matthews A, Dowey SJ. Plasma electrolysis for surface engineering. Surf Coat Technol 1999;122:73–93.
[8] Han Y, Xu KW. Photoexcited formation of bone apatite-like coatings on micro-arc oxidized titanium. J Biomed Mater Res A 2004;71:608–14.
[9] Frauchiger VM, Schlotting F, Gasser B, Textor M. Anodic plasma–chemical treatment of CP titanium surfaces for biomedical applications. Biomaterials 2004;25:593–606.
[10] Sul YT, Johansson CB, Petronis S, Krozer A, Jeong Y, Wennerberg A, et al. Characteristics of the surface oxides on turned and electrochemically oxidized pure titanium implants up to dielectric breakdown: the oxide thickness, micropore configurations, surface roughness, crystal structure and chemical composition. Biomaterials 2002;23:491–501.
[11] Sul YT. The significance of the surface properties of oxidized titanium to the bone response: special emphasis on potential biochemical bonding of oxidized titanium implant. Biomaterials 2003;24:3893–907.
[12] Giavaresi G, Fini M, Cigada A, Chiesa R, Rondelli G, Rimondini L, et al. Mechanical and histomorphometric evaluations of titanium implants with different surface treatments inserted in sheep cortical bone. Biomaterials 2003;24:1583–94.
[13] Yamashita K, Kitagaki K, Umegaki T. Thermal instability and proton conductivity of ceramic hydroxyapatite at high temperatures. J Am Ceram Soc 1995;78:1191–7.
[14] Wang W, Itoh S, Yamamoto N, Nagai A, Yamashita K. Electrical polarization of β-tricalcium phosphate ceramics. J Am Ceram Soc 2010;93:2175–7.
[15] Tanaka K, Nakamura S, Yoshida K, Hashimoto K, Toda Y, Yamashita K. Effects of electrical polarization on B-type carbonated hydroxyapatite. Phos Res Bull 2004;17:126–9.
[16] Kobayashi M, Saito H, Mase T, Sasaki T, Wang W, Tanaka Y, et al. Polarization of hybridized calcium phosphoaluminosilicates with 45S5-type bioglasses. Biomed Mater 2010;5:25001.
[17] Ueshima M, Nakamura S, Yamashita K. Huge-millicoulomb charge storage in ceramic hydroxyapatite by bimodal electric polarization. Adv Mater 2002;14:5915–7.
[18] Tarafder S, Banerjee S, Bandyopadhyay A, Bose S. Electrically polarized biphasic calcium phosphates: adsorption and release of bovine serum albumin. Langmuir Lett 2010;26:16625–9.
[19] Nakamura M, Nagai A, Hentunen T, Salonen J, Sekijima Y, Okura T, et al. Surface electric fields increase osteoblast adhesion through improved wettability on hydroxyapatite electra. ACS Appl Mater Interfaces 2009;1:2181–9.
[20] Bodhak S, Bose S, Bandyopadhyay A. Role of surface charge and wettability on early stage mineralization and bone cell–materials interactions of polarized hydroxyapatite. Acta Biomater 2009;5:2178–88.
[21] Itoh S, Nakamura S, Nakamura M, Shinomiya K, Yamashita K. Enhanced bone ingrowth into hydroxyapatite with interconnected pores by electrical polarization. Biomaterials 2006;27:5572–9.
[22] Kobayashi T, Itoh S, Nakamura S, Nakamura M, Shinomiya K, Yamashita K. Enhanced bone bonding of hydroxyapatite-coated titanium implants by electrical polarization. J Biomed Mater Res A 2007;82:145–51.
[23] Ruardy TG, Schakenraad JM, van der Mei HC, Busscher HJ. Adhesion and spreading of human skin fibroblasts on physiochemically characterized gradient surfaces. J Biomed Mater Res 1995;29:1415–23.
[24] Liao HH, Andersson AS, Sutherland D, Petronis S, Kasemi B, Thomsen P. Response of rat osteoblast-like cells to microstructured model surfaces in vitro. Biomaterials 2003;24:649–54.
[25] Yang B, Uchida M, Kim HM, Zhang XD, Kokubo T. Preparation of bioactive titanium metal via anodic oxidation treatment. Biomaterials 2004;25:1003–10.
[26] Wei DQ, Zhou Y, Jia DC, Wang YM. Characteristic and in vitro bioactivity of a microarc-oxidized TiO_2-based coating after chemical treatment. Acta Biomater 2007;3:817–27.
[27] Song WH, Jun YK, Han Y, Hong SH. Biomimetic apatite coatings on microarc oxidized titania. Biomaterials 2004;25:3341–9.
[28] Hanawa T, Kamiura Y, Yamamoto S, Kohgo T, Amemiya A, Ukai H, et al. Early bone formation around calcium-ion-implanted titanium inserted into rat tibia. J Biomed Mater Res 1996;36:131–6.
[29] Hansson S, Norton M. The relation between surface roughness and interfacial shear strength for bone-anchored implants. A mathematical model. J Biomech. 1999;32:829–36.
[30] Spurr RA, Myers H. Quantitative analysis of anatase–rutile mixture with an X-ray diffractometer. Anal Chem 1957;29:760–2.
[31] Huang P, Wang F, Xu K, Han Y. Mechanical properties of titania prepared by plasma electrolytic oxidation at different voltages. Surf Coat Technol 2007;201:5168–71.
[32] Lu G, Bernasek SL, Schwartz J. Oxidation of a polycrystalline titanium surface by oxygen and water. Surf Sci 2000;458:80–90.
[33] Hugenschmidt MB, Gamble L, Campbell CT. The interaction of H_2O with a TiO_2 (110) surface. Surf Sci 1994;302:329–40.
[34] Wang LQ, Baer DR, Engelhard MH, Shultz AN. The adsorption of liquid and vapor water on TiO_2 (110) surfaces: the role of defect. Surf Sci 1995;344:237–50.

[35] Dittrich Th, Weidmann J, Koch F, Uhlendorf I, Lauemann I. Temperature- and oxygen partial pressure-dependent electrical conductivity in nanoporous rutile and anatase. Appl Phys Lett 1999;75:3980–2.
[36] Sheng J, Fukami T, Karasawa J. X-ray photoemission spectroscopy (XPS) and thermally stimulated current (TSC) studies on the resistance degradation of iron-doped titania ceramics. J Am Ceram Soc 1998;81:260–2.
[37] Perron H, Vandenborre J, Domain C, Drot R, Roques J, Simoni E, et al. Combined investigation of water sorption on TiO_2 rutile (110) single crystal face. XPS vs. periodic DFT. Surf Sci 2007;601:518–27.
[38] Henderson MA, Epling WS, Peden CHF, Perkins CL. Insights into photoexcited electron scavenging processes on TiO_2 obtained from studies of the reaction of O_2 with OH groups adsorbed at electronic defects on TiO_2(110). J Phys Chem B 2003;107:534–45.
[39] Diebold U. The surface science of titanium dioxide. Surf Sci Rep 2003;48:53–229.
[40] Sakai N, Fujishima A, Watanabe T, Hashimoto K. Quantitative evaluation of the photoinduced conversion properties of TiO_2 thin film surfaces by the reciprocal of contact angle. J Phys Chem B 2003;107:1028–35.
[41] Mills A, Crow M. A study of factors that change the wettability of titania films. Int J Photoenergy 2008;470670.
[42] Jribi R, Barthel E, Bluhm H, Grunze M, Koelsch P, Verreault D, et al. Ultraviolet irradiation suppresses adhesion on TiO_2. J Phys Chem C 2009;113:8273–7.
[43] Takahashi K, Yui H. Analysis of surface OH groups on TiO_2 single crystal with polarization modulation infrared external reflection spectroscopy. J Phys Chem C 2009;113:20322–7.
[44] Mugele F, Baret JC. Electrowetting: from basics to applications. J Phys Condens Mater 2005;17:R705–74.
[45] Fan SK, Yang H, Wang TT, Hsu W. Asymmetric electrowetting moving droplets by a square wave. Lab Chip 2007;7:1330–5.
[46] Vallet M, Vallade M, Berge B. Limiting phenomena for the spreading of water on polymer films by electrowetting. Eur Phys J 1999;11:583–91.
[47] Raj B, Dhindsa M, Smith NR, Laughin R, Heikenfeld J. Ion and liquid dependent dielectric failure in electrowetting systems. Langmuir 2009;25:12387–92.

Langmuir

Article

pubs.acs.org/Langmuir

Wettability and Antifouling Behavior on the Surfaces of Superhydrophilic Polymer Brushes

Motoyasu Kobayashi,*[,†] Yuki Terayama,[‡] Hiroki Yamaguchi,[‡] Masami Terada,[†] Daiki Murakami,[†] Kazuhiko Ishihara,[∥] and Atsushi Takahara*[,†,‡,§]

[†]Japan Science Technology Agency, ERATO, Takahara Soft Interfaces Project

[‡]Graduate School of Engineering and [§]Institute for Materials Chemistry and Engineering, Kyushu University

[∥]Graduate School of Engineering, The University of Tokyo

Supporting Information

ABSTRACT: The surface wettabilities of polymer brushes with hydrophobic and hydrophilic functional groups were discussed on the basis of conventional static and dynamic contact angle measurements of water and hexadecane in air and captive bubble measurements in water. Various types of high-density polymer brushes with nonionic and ionic functional groups were prepared on a silicon wafer by surface-initiated atom-transfer radical polymerization. The surface free energies of the brushes were estimated by Owens-Wendt equation using the contact angles of various probe liquids with different polarities. The decrease in the water contact angle corresponded to the polarity of fluoroalkyl, hydroxy, ethylene oxide, amino, carboxylic acid, ammonium salt, sulfonate, carboxybetaine, sulfobetaine, and phosphobetaine functional groups. The poly(2-perfluorooctylethyl acrylate) brush had a low surface free energy of approximately 8.7 mN/m, but the polyelectrolyte brushes revealed much higher surface free energies of 70−74 mN/m, close to the value for water. Polyelectrolyte brushes repelled both air bubbles and hexadecane in water. Even when the silicone oil was spread on the polyelectrolyte brush surfaces in air, once they were immersed in water, the oil quickly rolled up and detached from the brush surface. The oil detachment behavior observed on the superhydrophilic polyelectrolyte brush in water was explained by the low adhesion force between the brush and the oil, which could contribute to its excellent antifouling and self-cleaning properties.

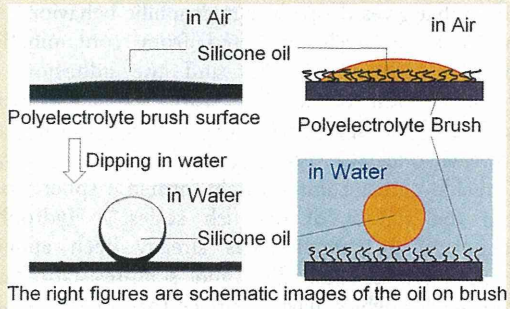

The right figures are schematic images of the oil on brush in the left photographs.

INTRODUCTION

Hydrophilic surfaces and interfaces have attracted much attention because of their applications in water lubrication,[1] antifouling and nonbiofouling surfaces,[2] and biocompatible materials.[3] The surfaces of living cells, cartilage, the vitreous body of eyes, and synovial joints are all hydrophilic surfaces and interfaces consisting of polyelectrolytes that afford excellent biolubrication.[4,5] One of the useful artificial methods of producing a hydrophilic surface is grafting a polymer onto a solid surface. With this method, the wettability and hydrophilicity can be tuned by the chemical structure of the polymer and remain stable for a long period of time because of the covalent anchoring of the polymers to the substrate.

Recently, many types of hydrophilic polymer surfaces with suitable wettability and antifouling properties, especially bioantifouling, have been proposed and prepared by the surface-initiated controlled radical polymerization of vinyl monomers with specially designed hydrophilic functional groups, leading to densely grafted polymers on the solid surface, so-called polymer brushes.[6] For example, the poly(oligoethyleneglycol methacrylate) brush[7] and polysulfobetaine brushes[8,9] have antifouling and nonbiofouling surfaces with good wettability. Théodoly et al. prepared well-anchored polystyrene-*block*-poly(acrylic acid) on a polystyrene film to form a poly(acrylic acid) brush that exhibited wetting transition behavior from partial to total wetting according to deposition conditions.[10] Spruijt et al. achieved surface wettability control of a poly(2-(methacryloyloxy)ethyltrimethylammonium chloride) (PMTAC) brush by changing the counterions and electrode potentials.[11] Superhydrophilic poly[2-(methacryloyloxy)ethyl phosphorylcholine] (PMPC) is well known as an excellent biocompatible and blood-compatible polymer,[12] and its grafted surface shows low friction in aqueous media and humid air.[13,14]

Self-cleaning often depends on the ability of superhydrophobic surfaces to wash out oily contamination particles with water drops flowing on a surface.[15] For example, the leaves of the lotus plant have a typical self-cleaning surface provided by an intrinsic hierarchical structure with randomly oriented hydrophobic wax bosses.[16] Oleophobicity and self-cleaning behavior can also be provided by superhydrophilic surfaces in the wetted state by water.[17−19] For example, fish can maintain a

Received: March 13, 2012
Revised: April 13, 2012
Published: April 16, 2012

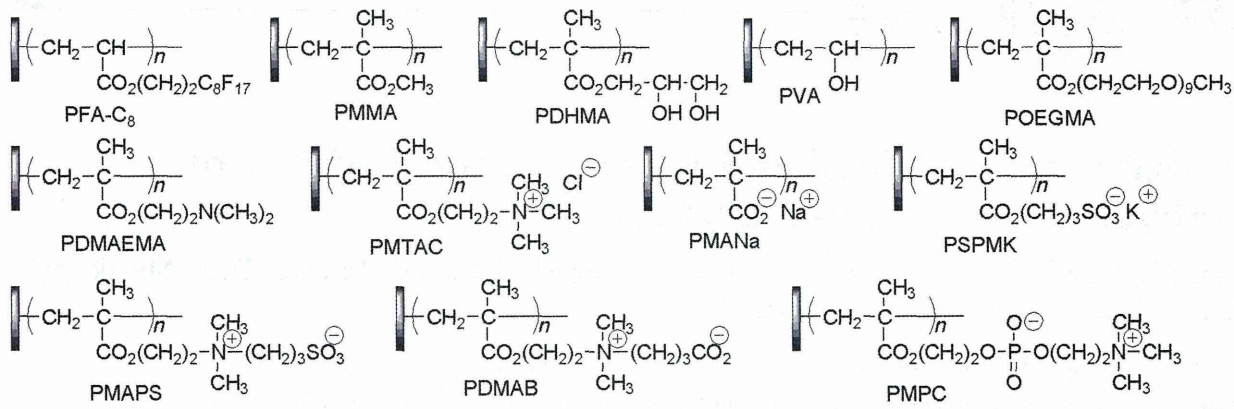

Figure 1. Chemical structures and abbreviations of polymer brushes.

clean body surface even in oil-polluted water. Fish scales are composed of calcium phosphate, protein, and a thin layer of mucus that gives them their hydrophilic behavior, and they are known to be well protected from contamination by oil pollution, marine fouling, and the adhesion of marine organisms. Liu et al. demonstrated that a drop of 1,2-dichloroethane spreads on the surface of fish scales in air. However, once the scales were immersed in water, a drop of 1,2-dichloroethane immediately formed a sphere to flow away from the surface of the fish scales.[20] Hydrophilic nanotechnology in ceramics has already been applied to the development of new dirt- and stain-resistant materials for exterior tiles, which have a surface that absorbs moisture from the air to form a thin water layer.[21] This layer allows dirt adsorbed on the tile surface to be washed off by rainfall. Therefore, it is expected that self-cleaning surfaces can be artificially fabricated by grafting hydrophilic brushes onto substrates.

In this study, both hydrophobic and hydrophilic polymer brushes bearing nonionic and ionic functional groups were prepared by surface-initiated atom-transfer radical polymerization (SI-ATRP) to compare their wettabilities and antifouling properties on the basis of the contact angles of water in air and captive air bubbles as well as hexadecane and silicone oil droplets in water. The oil detachment behavior on swollen hydrophilic brush surfaces in water was explained by the adhesion force between the brush and oil.

In addition, the surface free energies of the brushes were also estimated by different calculation methods, such as Owens' method[22] and the acid–base theory proposed by Fowkes,[23,24] and by van Oss, Chaudhury, and Good.[25] These methods are still being discussed in the field of surface science[26−28] because of the discrepancies in the surface free energy, even that of poly(methyl methacrylate) (PMMA), given by individual methods. However, the surface free energy is scientifically important to an understanding of surface characterization. We tried here to understand the fundamental wettability and antifouling behavior of brush surfaces based on the surface free energy.

EXPERIMENTAL SECTION

Materials. Copper(I) bromide (CuBr, Wako Pure Chemicals) was purified by successive washing with acetic acid and ethanol and was dried under vacuum. Methyl methacrylate (MMA), vinyl acetate (VAc), ethyl iodoisobutylate, and ethyl 2-bromoisobutylate (EB) purchased from Tokyo Chemical Inc. (TCI) were distilled before use. (−)Spartein (Nacalai Tesque) was distilled under reduced pressure and then stored as an anisole solution. Hexadecane (Nacalai Tesque), diiodomethane (Nacalai Tesque), 2,2′-bipyridyl (bpy, Aldrich), 4,4′-dimethyl-2,2′-bipyridyl (Me_2bpy, Aldrich), 4,4′-dinonyl-2,2′-bipyridyl (C_9bpy, Aldrich), 2,2,2-trifluoroethanol (TFE, Acros, 99.9%), and 2,2′-azobis(4-methoxy-2,4-dimethyl valeronitrile) (V-70, Aldrich) were used as received. 2-Perfluorooctylethyl acrylate (FA-C_8) monomer was kindly donated by Daikin Co. Ltd. and was purified by distillation under reduced pressure repeatedly to remove other types of monomer, such as 2-(perfluorodecyl)ethyl acrylate. The purity of FA-C_8 was over 98% by gas chromatography. 2-(*N*,*N*-Dimethylamino)ethyl methacrylate (DMAEMA, TCI) was distilled in the presence of calcium hydride under reduced pressure and was diluted with acetone for storage in a 2.5 M solution. Oligoethylene glycol methacrylate (OEGMA, Aldrich) with nine units of ethylene glycol on the side chain was passed through an aluminum column to remove the stabilizer prior to use. Sulfobetaine-type monomer was freshly synthesized before use by the reaction of DMAEMA and 1,3-puropanesultone and purified by recrystallization in hexane solution to give 3-[dimethyl(2′-methacryloyloxyethyl)ammonio]propanesulfonate (MAPS) as a white powder. MPC monomer was prepared using a previously reported procedure.[12] The other methacrylate monomers, such as methacrylic acid sodium salt (MANa, Wako Chemicals), 3-sulfopropyl methacrylate potassium salt (SPMK, Aldrich), and 4-[dimethyl(2′-methacryloyloxyethyl)ammonio]butanoate (DMAB, Otsuka Chemical Co.), were used as received without any purification. A commercially available MTAC aqueous solution (Aldrich, 80%) was concentrated using a vacuum pump to remove water and then dissolved in TFE. The MTAC/TFE solution was purified by alumina column chromatography and membrane filtration. Deionized water for contact angle measurement was purified with a NanoPure Water system (Millipore Inc.).

Preparation of Polymer Brushes. All brush samples were prepared by the grafting-from method using SI-ATRP from a silicon wafer immobilized with a surface initiator. The surface initiator, (2-bromo-2-methyl)propionyloxyhexyl trimethoxysilane (BHM), was synthesized via the hydrosilylation reaction of 5′-hexenyl (2-bromo-2-methyl)propionate and trimethoxysilane in the presence of Karstedt catalyst[29] and immobilized on a purified silicon wafer by the chemical vapor adsorption method.[30,31] The chemical structures of polymer brushes were illustrated in Figure 1. An unbound initiator as a sacrificial initiator is necessary to control the degree of polymerization and to estimate the number-average molecular weights (M_n) of the resulting polymer.[32] A typical SI-ATRP of MTAC was performed as follows.[33] A few sheets of the BHM-immobilized silicon wafers, 4.0 mL of MTAC/TFE solution (2.0 M), and 0.30 mL of 2-propanol were placed in a well-dried glass tube with a stopcock and then degassed using a freeze–thaw process that was repeated three times. A catalyst solution containing CuBr (0.020 mmol), bpy (0.040 mmol), and EB (0.020 mmol) diluted with TFE was injected into the monomer solution. The resulting reaction mixture was degassed again by repeated freeze–thaw cycles to remove the oxygen and then stirred in an oil bath at 333 K for 16 h under argon, which simultaneously

dx.doi.org/10.1021/la301033h | *Langmuir* 2012, 28, 7212−7222

generated poly(MTAC) brushes from the substrate and free (unbound) poly(MTAC) from EB. The reaction was stopped by opening the glass vessel to air at 293 K. The reaction mixture was poured into THF to precipitate the free polymer and unreacted MTAC. The silicon wafers were washed with methanol using a Soxhlet apparatus for 12 h to remove the free polymer absorbed on their surfaces and dried under nitrogen gas at room temperature.

The PMPC brush was synthesized in a similar manner using CuBr and Me_2bpy in methanol at 303 K for 12 h.[13] SI-ATRP of the FA-C_8 brush was conducted in the presence of CuBr and C_9bpy at 383 K for 72 h under an argon atmosphere to generate the PFA-C_8 brush on the silicon substrate.[34] The PMMA brush was prepared by SI-ATRP using a CuBr/(-)spartein catalyst in anisole at 333 K for 3 days. A poly(2,3-dihydroxypropyl methacrylate) (PDHMA) brush was prepared by SI-ATRP of (2,2-dimethyl-1,3-dioxolan-4-yl)methyl methacrylate (DMM) and successive acid hydrolysis.[35] The PVA brush was prepared by surface-initiated iodide-transfer polymerization of VAc and successive acid hydrolysis.[36] SI-ATRP of OEGMA was performed using CuBr and bpy in methanol at 303 K for 5 days. DMAEMA underwent SI-ATRP by the CuBr/pentamethyldiethyletriamine system in acetone at 303 K for 24 h. SI-ATRP of MAPS was performed in TFE using CuBr and bpy at 303 K for 24 h to give the PMAPS brush.[37] MANa was polymerized in an aqueous solution at pH 8.3 (2.2 M of MANa) using CuBr and Me_2bpy at 298 K for 3 h.[38] SI-ATRP of SPMK was carried out in methanol/water (5/2 v/v, 1.7 M SPMK) at 298 K for 15 h using a reaction system consisting of SPMK/CuBr/$CuBr_2$/Me_2bpy in the following molar ratio: 200/2/0.4/4.[39] The PDMAB brush was prepared by SI-ATRP in the presence of CuBr and bpy in methanol at 333 K for 48 h.

Measurements. The molecular weight and molecular weight distribution of the unbound polymers were estimated by size exclusion chromatography (SEC) using a Shimadzu HPLC system equipped with a multiangle light-scattering detector (MALS, Wyatt Technology DAWN-EOS, 30 mW GaAs linearly polarized laser, wavelength λ = 690 nm) and a refractive index detector (Shimadzu RID-10A, tungsten lamp, wavelength 470–950 nm). The Rayleigh ratio at a scattering angle of 90° was based on that of pure toluene at a wavelength of 632.8 nm at 25 °C. SEC of PMPC was performed with three polystyrene gel columns connected to two super AW3000 and super AW4000 (Tosoh Bioscience) using water containing 0.01 M LiBr as an eluent at a rate of 0.5 mL/min at 313 K. PMAPS required polymethacrylate-based TSKgel columns consisting of G6000PW_{XL}, G5000PW_{XL}, and G3000PW_{XL} (Tosoh Bioscience) using a 200 mM NaCl aqueous solution as an eluent at a rate of 0.8 mL/min at 313 K. In the case of PMTAC, three polystyrene gel columns of Tosho G3000PW_{XL}-CP and two polystyrene gel columns of Tosho G5000PW_{XL}-CP were used with an acetic acid aqueous solution (500 mM) containing sodium nitrate (200 mM) as an eluent at a rate of 0.6 mL/min. SEC of PFA-C_8 was conducted with three gel columns of α6000, α5000, and α4000 (Tosoh Bioscience) using 1,1,1,3,3,3-hexafluoro-2-propanol as an eluent at a rate of 0.5 mL/min. The SEC of PMMA was measured on three gel columns of G5000H_{XL}, G4000H_{XL}, and G3000H_{XL} (Tosoh Bioscience) using THF as an eluent at a flow rate 1.0 mL/min at 313 K. DMF containing 0.01 M LiBr was employed for PDMM, PVAc, PDMAEMA, and POEGMA. Calibration curves were prepared with a series of PMMA standards.

The thickness of the polymer brushes immobilized on a silicon wafer in air (the relative humidity was ca. 45%) was determined by a MASS-102 spectroscopic ellipsometer (Five Lab Co.) with a xenon arc lamp (wavelength 380–890 nm) at a fixed incident angle of 70°. The thickness was also measured by AFM of a partially scratched brush film under vacuum to prevent the influence of moisture. AFM observation was done with E-Seep with an SPI 3800N controller (SII NanoTechnology, Inc.) using a silicon nitride (Si_3N_4) integrated tip on a commercial triangular 200 mm cantilever (Olympus Co., Ltd.) with a spring constant of 0.09 N m^{-1}.

The static and dynamic contact angles were recorded with a DSA10 Mk2 (Krüss, Inc.) drop shape analysis system equipped with a video camera using an inclinable plane. A 2.0 μL droplet of water, diiodomehane, ethylene glycol, formamide, dimethylsulfoxide, or hexadecane was placed on the surface using a micropipet to measure the static contact angle (Figure 2a). The surface free energy and parameters of these probe liquids are listed in Table 1. In an inclinable plane, the sample on the stage was tilted at 2 deg/s until a 30 μL water droplet began to slide down the sample surface. Subsequently, the advancing contact angle (θ_A), the receding contact angle (θ_R), and the sliding angle (θ_S) were determined (Figure 2b).[40] All of these evaluations were conducted in ambient air at room temperature (approximately 298 K). The relative humidity was approximately 40%. The contact angles of a captive air bubble and hexadecane in water were measured on the brush substrate facing downward in a square transparent glass vessel filled with deionized water or hexadecane-saturated water. The air bubble or hexadecane droplet (10 μL) was released from beneath the brush substrate using a microsyringe, as shown in Figure 2c.

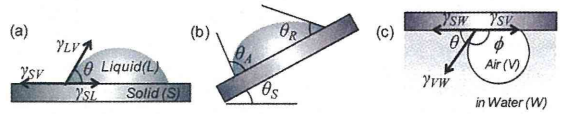

Figure 2. Definitions of static θ, advancing θ_A, receding θ_R, and sliding θ_S contact angles of liquid on a solid surface in air and the contact angle ϕ of an air bubble in water.

RESULTS AND DISCUSSION

Surface Modification by Polymer Brushes. SI-ATRP smoothly proceeded on the BHM-immobilized silicon substrate to give PFA-C_8, PMMA, PDMM, PDMAEMA, PMTAC, and PMPC brushes. The corresponding unbound polymers were also generated from the sacrificial free initiator simultaneously. The M_n values of the unbound polymer brushes were determined with an SEC-MALS system to be 30 000–150 000, which were expected to be the same as those of the corresponding brushes.[33,37,41,42] The thickness of a dried polymer brush film, L, was determined by ellipsometry. Most of the brushes were thicker than 40 nm, except for the PVA brush, which was 20 nm in thickness. The graft density of a brush, σ, was theoretically estimated with the following equation by assuming that the reflective index was uniform in the thin brush layer

$$\sigma = \frac{dL_d N_A \times 10^{-21}}{M_n} \quad (1)$$

where d and N_A are the assumed density of the bulk polymer at 293 K and Avogadro's number, respectively. For example, the σ values of PFA-C_8, PMMA, PDMM, PDMAEMA, and PMPC brushes were 0.15, 0.56, 0.36, 0.40, and 0.23 chains/nm^2, respectively. AFM observation revealed that a homogeneous polymer layer was formed on the substrate and that the surface roughness was 0.8–1.5 nm in a dry state over a 5 × 5 μm^2 scanning area. Hydrolysis of the PDMM brush under mildly acidic conditions produced a PDHMA brush without any elimination of brushes from the substrate.[35] A PVA brush was prepared by the surface-initiated iodide-transfer polymerization of VAc and subsequent acid hydrolysis.[36] Aqueous SI-ATRP of MANa proceeded very quickly in spite of the absence of free initiator and resulted in a polymer brush of 200 nm thickness within a few hours.[38] Similarly, SI-ATRP of SPMK and DMAB were conducted without sacrificial free initiators to result in polyelectrolyte brushes with thicknesses of up to 100 nm.

dx.doi.org/10.1021/la301033h | Langmuir 2012, 28, 7212–7222

Table 1. Surface Free Energies and the Acidic and Basic Components of the Liquids Employed[a]

liquid (symbol)[refs]	γ_{LV} (mN/m)	γ_{LV}^{d} (γ_{LV}^{LW}) (mN/m)	γ_{LV}^{p} (γ_{LV}^{AB}) (mN/m)	γ_{LV}^{-} (mN/m)	γ_{LV}^{+} (mN/m)	γ_{LW} (mN/m)
water (W)[44−46]	72.80	21.80	51.00	25.50	25.50	
water (W*)[26]	72.90	22.50	50.40	10.80	58.80	
formamide (F)[43]	58.10	35.50	22.60	11.30	11.30	
formamide (F*)[26]	57.83	32.10	25.73	59.10	2.80	
diiodomethane (I)	50.80	49.50	1.30	0.65	0.65	41.6
diiodomethane (I*)[26]	50.98	50.90	0.08	0.035	0.47	48.5
ethylene glycol (E)[43]	48.00	29.00	19.00	47.00	1.92	
ethylene glycol (E*)[26]	48.10	31.20	16.90	34.00	2.10	
dimethylsulfoxide (D)[43,44]	44.00	36.00	8.00	32.00	0.50	
dimethylsulfoxide (D*)[26]	44.17	34.40	9.77	19.90	1.20	
hexadecane (HD)[44]	27.6	27.6	0.0	0.0	0.0	53.7

[a]The surface free energy of probe liquids (γ_{LV}) and their components attributed to Liftshitz−van der Waals (γ_{LV}^{LW}), the acid−base components (γ_{LV}^{AB}), the electron-donor (γ_{LV}^{-}), and the electron-acceptor (γ_{LV}^{+}) interactions. γ_{LW} is the interfacial free energy of the probe liquid/water.

Table 2. Contact Angle of Various Liquids on the Surfaces of the Polymer Brushes[a]

polymer brushes	water (deg)	diiodomethane (deg)	ethylene glycol (deg)	dimethylsulfoxide (deg)	formamide (deg)	hexadecane (deg)
PFA-C_8	121 ± 0.8	100 ± 0.8	102 ± 0.6	90 ± 1.1	103 ± 1.4	74 ± 1.1
PMMA	74 ± 1.1	36 ± 1.9	49 ± 1.5	22 ± 1.9	60 ± 0.9	<3
PMANa	31 ± 1.4	44 ± 1.4	8 ± 1.1	<3	15 ± 0.8	<3
PMTAC	12 ± 1.3	35 ± 1.5	8 ± 1.9	9 ± 1.8	10 ± 0.9	<3
PSPMK	7 ± 1.6	39 ± 1.1	11 ± 1.7	3 ± 0.5	5 ± 0.9	<3
PMAPS	11 ± 2.1	30 ± 1.8	5 ± 0.8	17 ± 0.9	15 ± 1.3	<3
PMPC	<3	27 ± 1.8	7 ± 1.4	<3	6 ± 1.2	<3

[a]All of the static contact angles were measured with a 2 μL droplet.

Table 3. Contact Angles on Nonionic-Type Polymer Brushes

		PFA-C_8 (deg)	PMMA (deg)	PDHMA (deg)	PVA (deg)	PEGMA (deg)	PDMAEMA (deg)
water	θ: static[a]	121 ± 0.8	74 ± 1.1	60 ± 1.8	45 ± 1.5	44 ± 1.7	56 ± 1.2
	θ_A: advancing[b]	127 ± 0.9	99 ± 1.0	76 ± 2.1	71 ± 0.9	89 ± 0.8[c]	78 ± 1.8
	θ_R: receding[b]	110 ± 1.1	58 ± 0.9	18 ± 1.9	20 ± 0.8	21 ± 0.9[c]	27 ± 1.0
	θ_S: sliding[b]	6 ± 1.2	43 ± 1.7	80 ± 0.6	50 ± 1.2	60 ± 1.5[c]	62 ± 1.3
diiodomethane	θ: static[a]	100 ± 0.8	36 ± 1.9	40 ± 1.8	25 ± 1.1	18 ± 0.9	38 ± 0.9
hexadecane	θ: static[a]	74 ± 1.1	<3	6 ± 0.5	10 ± 0.9	16 ± 1.1	<3
air bubble in water	ϕ: static[d]	59 ± 1.0	104 ± 1.3	145 ± 1.5	142 ± 1.2	142 ± 0.9	138 ± 1.8
hexadecane in water	ϕ: static[d]	<3	89 ± 1.1	108 ± 1.0	119 ± 1.0		

[a]All the static contact angles were measured with a 2 μL droplet. [b]Dynamic contact angles were measured with 30 μL of water. [c]40 μL. [d]ϕ is the supplementary angle for the contact angle of an air bubble (10 μL) in water.

Surface Wettability of Nonionic Polymer Brushes. The water contact angles of polymer brush surfaces are summarized in Tables 2−4. The contact angle measurements were performed at room temperature (298 K) using a contact angle goniometer equipped with video camera recording system operated by software for drop-shape analysis. Three different probe liquids (Milli-Q water, ethylene glycol, and diiodomethane) were used.

Figure 2 illustrates the schematic view of the (a) static and (b) dynamic contact angles of the liquid droplets in air and (c) the contact angle of the air bubble captured on a solid surface in water. The surface free energy γ_{SV} for a solid (S) in contact with saturated vapor (V) is described by the well-known Young equation using the interfacial free energy γ_{SL} at the brush and liquid (L) interfaces

$$\gamma_{SV} = \gamma_{SL} + \gamma_{LV} \cos\theta \quad (2)$$

where γ_{LV} and θ are the surface free energy and the contact angle of the liquid, respectively. When the liquid is water (W), the surface and interfacial free energies are described as γ_{WV} and γ_{SW}. The surface free energy can be described by the extended Fowkes equation using the dispersion force (γ^d) and polar force (γ^p) components.[23]

$$\gamma_{SL} = \gamma_{SV} + \gamma_{LV} - 2(\gamma_{SV}^{d}\gamma_{LV}^{d})^{1/2} - 2(\gamma_{SV}^{p}\gamma_{LV}^{p})^{1/2} \quad (3)$$

where the surface free energy γ_{SV} consists of γ_{SV}^{d} and γ_{SV}^{p}.

$$\gamma_{SV} = \gamma_{SV}^{d} + \gamma_{SV}^{p} \quad (4)$$

Then, eqs 2 and 3 give the Owens-Wendt equation (eq 5):[22]

$$(1 + \cos\theta)\gamma_{LV} = 2(\gamma_{SV}^{d}\gamma_{LV}^{d})^{1/2} + 2(\gamma_{SV}^{p}\gamma_{LV}^{p})^{1/2} \quad (5)$$

Therefore, the surface free energy of the polymer brush can be calculated by the contact angles of two types of liquids with different γ^d and γ^p values, for example, water and diiodomethane, using eq 5. Table 5 displays the interfacial free energies of the polymer brushes versus vapor γ_{SV} and water γ_{SW} evaluated by Owens' method. The γ_{SW} estimated by the water contact angle in the vapor phase is described as γ_{SW}^{V} in Table 5 to distinguish it from γ_{SW}^{W} estimated by the captive bubble

dx.doi.org/10.1021/la301033h | Langmuir 2012, 28, 7212−7222

technique in water, as described later. The surface free energy components of probe liquids attributed to the Liftshitz–van der Waals (γ_{LV}^{LW}) and acid–base components (γ_{LV}^{AB}) and the electron-donor (γ_{LV}^{-}) and electron-acceptor (γ_{LV}^{+}) interactions are listed in Table 1.[43−46]

As shown in Table 3, the PFA-C_8 brush with a broad molecular weight distribution had the highest water contact angle of the brushes, which was 121°, and the lowest surface free energy of 8.6 mN/m for a series of brushes. Typical photographs of water and hexadecane droplets on the surfaces of nonionic-type polymer brushes are displayed in Figure 3.

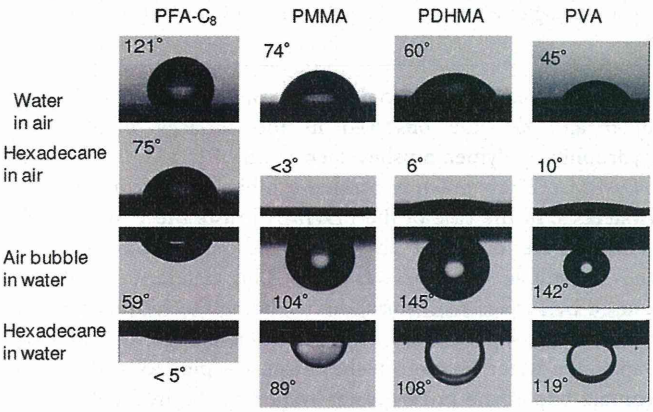

Figure 3. Photographs (side view) of water and hexadecane droplets on polymer brushes in air and an air bubble and hexadecane in contact with the brush surface in water.

The contact angle of hexadecane on the PFA-C_8 brush surface was 74°, implying oleophobic behavior. The low surface tension was caused not only by the low polarity of the C–F bond[47] and the weak molecular interactions of fluorocarbons but also by the unique aggregation structure of perfluorooctyl chains at the brush surface.[48−51] Perfluorooctyl chains at the outermost surface were oriented perpendicular to the substrate surface, forming a densely packed structure to afford a stable hydrophobic surface.[48]

The contact angle of the PFA-C_8 brush surface was influenced by the brush thickness and molecular weight dispersity.[52] When the brush thickness was increased from 4 to 20 nm, the static water contact angle gradually increased from 107 to 120°, which was related to the molecular aggregation state of the perfluoroalkyl (R_f) chains. The orientation of R_f chains at the outermost surface in the PFA-C_8 brush that was thicker than 12 nm was confirmed by a grazing incident wide-angle X-ray diffraction measurement, whereas no diffraction peaks were detected from the thinner PFA-C_8 brush film. The brush that was thicker than 20 nm had an X-ray diffraction pattern caused by the lamellar structure composed of the R_f groups.[34] The densely packed structure of the R_f groups contributed to the reduction in the surface free energy, which was the case for the dependency of the water contact angle on the brush thickness. In this work, a series of polymer brushes with sufficient thickness were prepared to obtain stable contact angles to estimate their surface free energies and specific characteristics.

Polymer brushes with polar functions such as carbonyl, hydroxy, ether, and amino groups had lower water contact angles. PDHMA, PVA, PEGMA, and PDMAEMA are all water-soluble polymers. However, the corresponding polymer brushes had different contact angles depending on their hydrophilicity. Even though hydroxy groups were attached to the side chain or main chain, PDHMA and PVA brushes had relatively high contact angles of 63 and 45°, respectively. Much higher sliding angles and asymmetric drops with high θ_A and low θ_R were observed for PDHMA and PVA brushes than for the other brushes. A water droplet on the PDHMA brush surface did not slide until a tilting angle of 80°, whereas a water droplet on the PMMA brush began to slide when the plate was tilted to 18°.

Generally, contact angle hysteresis on the polymer surface reflects the reorientation of surface polymer chains,[53,54] the rearrangement of the surface structure,[55] topological roughness,[56,57] chemical heterogeneity,[58] and surface defects.[59] When the PDHMA brush was exposed to air (or vapor), the hydrophobic α-methyl group attached to the polymer backbone could be oriented toward the top surface to minimize the interfacial free energy. Alternatively, once the brush was exposed to water, the polar functional groups on the side chain would orient themselves toward the water interface. The strong hydrogen bonding interaction among the hydroxy group and water molecules contributed to a low θ_R, and the α-methyl groups formed a hydrophobic barrier at the air/brush interface, preventing wetting to give a higher θ_A. Large hysteresis and θ_S were also observed for the PEGMA and PDMAEMA brushes. The water contact angle hysteresis is related to the contact angles of air bubbles in water. In addition, the hydrophilic polymer brushes with high graft density were hydrated in water, forming an extended conformation as a result of the osmotic pressure. Therefore, the hydration free energy at the edge of the brush where the water meets the vapor phase should be considered in the study of the water contact angle of a brush,[60,61] as described below.

The contact angles ϕ of the air bubble and hexadecane in water were measured by Hamilton's method (Figure 2c).[62,63] The interfacial energies for brush–water vapor (γ_{SV}), hydrated brush–water (γ_{SW}), and brush–hexadecane (γ_{SO}) were also estimated by Andrade's protocol.[64] Young's equation gives

$$\gamma_{SV} - \gamma_{SW} = \gamma_{WV} \cos\theta \tag{6}$$

where θ is the contact angle of the air bubble filled with water vapor for which Young's equation holds, as shown in Figure 2c. When a drop of hexadecane is in contact with a brush–water interface with an angle of ϕ, the equation should be

$$\gamma_{SW} = \gamma_{SO} + \gamma_{OW} \cos\phi \tag{7}$$

where γ_{OW} is the interfacial energy for hexadecane–water. Hamilton and Andrade et al. assumed the following treatment for the interfacial free energy between hexadecane/solid and solid/water proposed by Fowkes et al.[65] and Tamai et al.[66]

$$\gamma_{SO} \approx \gamma_{SV} + \gamma_{OV} - 2(\gamma_{SV}^{d}\gamma_{OV}^{d})^{1/2} - I_{SO} \tag{8}$$

$$\gamma_{SW} \approx \gamma_{SV} + \gamma_{WV}' - 2(\gamma_{SV}^{d}\gamma_{WV}^{d})^{1/2} - I_{SW} \tag{9}$$

where γ_{WV}' is the surface tension of hexadecane-saturated water and I_{SO} and I_{SW} are polar interaction parameters for the solid/hexadecane and solid/water interfaces, respectively. Parameter I_{SO} is zero because hexadecane is completely nonpolar. γ_{WV}' is approximated to be the same as γ_{WV} because of the extremely low solubility of hexadecane in water. Combining eqs 7–9 gives

$$I_{SW} = \gamma_{WV} - \gamma_{OV} - \gamma_{OW}\cos\phi + 2(\gamma_{SV}^{d}\gamma_{OV}^{d})^{1/2} - 2(\gamma_{SV}^{d}\gamma_{WV}^{d})^{1/2} \tag{10}$$

dx.doi.org/10.1021/la301033h | Langmuir 2012, 28, 7212–7222

Table 4. Contact Angles on Polyelectrolyte Brushes

		PMANa (deg)	PMTAC (deg)	PSPMK (deg)	PDMAB (deg)	PMAPS (deg)	PMPC (deg)
water	θ: static[a]	31 ± 1.4	12 ± 1.3	7 ± 1.6	16 ± 1.4	11 ± 2.1	<3
	θ_A: advancing[b]	66 ± 1.0	50 ± 1.2	32 ± 2.0	18 ± 1.9	24 ± 1.8	13 ± 0.9
	θ_R: receding[b]	13 ± 0.8	12 ± 0.7	3 ± 0.8	6 ± 1.1	<3	<3
	θ_S: sliding[b]	45 ± 1.5	28 ± 2.1	12 ± 1.0	6 ± 2.0	11 ± 2.1	15 ± 1.4
diiodomethane	θ: static[a]	39 ± 1.4	35 ± 1.5	39 ± 1.1	40 ± 1.8	30 ± 1.8	27 ± 1.8
hexadecane	θ: static[a]	<3	<3	<3	<3	12 ± 1.8	<3
ethylene glycol	θ: static[a]	8 ± 1.1	8 ± 1.9	11 ± 1.7	8 ± 1.9	5 ± 0.8	7 ± 1.1
air bubble in water	ϕ: static[d]	154 ± 0.7	156 ± 1.0	160 ± 1.8	148 ± 1.8	155 ± 1.9	170 ± 0.8
hexadecane in water	ϕ: static[d]	170 ± 0.8	151 ± 1.8	176 ± 1.1	158 ± 1.2	175 ± 0.9	175 ± 0.6

[a]All the static contact angles were measured with a 2 μL of droplet. [b]Dynamic contact angles were measured with 30 μL of water. [c]10 μL. [d]ϕ is the supplementary angle for the contact angle of an air bubble (10 μL) in water.

From eq 9, it can be shown that

$$I_{SW} = \gamma_{WV} + (\gamma_{SV} - \gamma_{SW}) - 2(\gamma_{SV}^{d}\gamma_{WV}^{d})^{1/2} \quad (11)$$

The captive bubble method gives a value of $(\gamma_{SV} - \gamma_{SW})$ from eq 6. Because γ_{WV} = 72.8 mN/m, γ_{WV}^{d} = 21.8 mN/m, γ_{OV} = γ_{OV}^{d} = 27.6 mN/m, and γ_{OW} = 53.7 mN/m, I_{SW} and γ_{SV}^{d} can be calculated by a combination of eqs 10 and 11. γ_{SV}^{p} can be determined if

$$I_{SW} \approx 2(\gamma_{SV}^{p}\gamma_{WV}^{p})^{1/2} \quad (12)$$

γ_{SV} was given by γ_{SV}^{d} and γ_{SV}^{p} using eq 4. The interfacial energy for the brush–water interface was found with eq 6 and is listed in Table 5 as γ_{SW}^{W}.

Table 5. Surface Free Energy of Polymer Brushes Determined by Owens-Wendt Protocol

polymer brushes	γ_{SV} (mN/m)[a]	γ^{d} (mN/m)	γ^{p} (mN/m)	γ_{SW}^{V} (mN/m)[b]	γ_{SW}^{W} (mN/m)[c]
PFA-C_8	8.7	8.4	0.3	46.2	54.8
PMMA	43.8	37.5	6.2	23.7	13.6
PDHMA	48.1	33.0	15.1	11.7	9.3
PVA	59.6	37.5	22.1	8.1	3.8
PEGMA	61.2	39.6	21.6	8.8	
PDMAEMA	50.8	33.4	17.4	10.1	
PMANa	66.6	29.5	37.1	4.3	0.7
PMTAC	72.4	30.5	41.9	0.1	0.1
PSPMK	72.9	28.5	44.4	0.7	0.1
PDMAB	70.8	28.3	42.5	0.8	0.9
PMAPS	73.1	32.5	40.6	1.7	0.7
PMPC	74.5	33.5	41.0	0.2	0.1

[a]Determined with contact angles of water and diiodomethane droplets using parameters W and I in Table 1. [b]The interface energy for brush–water evaluated with the water contact angle in air. [c]The interfacial energy for brush–water evaluated with the captive bubble technique in water.

Photographs of air bubbles and hexadecane droplets attached to the brush surfaces in water are also shown in Figure 3. The contact angle ϕ of the air bubble on the PFA-C_8 brush in water was 59°, which corresponded to the supplementary angle of the water contact angle (θ = 121°) in air to 180°. If there is no surface reorganization, then the sum of ϕ values for the air bubble in water and θ for the water droplet in air should be 180°. The PMMA brush surface, for example, showed θ = 74° for the water contact angle and ϕ = 104° for the air bubble contact angle in water.

However, larger total angles than 180° for the combination of θ and ϕ were observed in the surfaces of nonionic hydrophilic polymer brushes such as the PDHMA, PVA, and PDAEMA. These polymer brushes exhibited large contact angle hysteresis. In the case of the PDHMA brush, the contact angle θ of the water droplet in air was 60° and the contact angle ϕ of the air bubble in water was 145°. This difference might be caused by surface reorganization, including the reorientation of functional groups after the environmental change. Under air or vapor, the water droplet on the brush was pinned at the triple contact line of the brush–water–vapor by the hydrophobic α-methyl groups, preventing wetting and leading to a higher magnitude of θ. In water, the PDHMA brush formed a swollen structure by hydration. When the air bubble was in contact with the hydrated brush surface, a conformational change in the polymer chain occurred to reduce the interfacial free energy between the brush and air. However, it would be hard to exclude the water molecule from the hydrophilic polymer because of the strong hydration force between water and the polar functional groups. A similar situation occurs at the receding water line on the tilted brush substrate in air. As a result, ϕ had a value close to 180° − θ_R, not 180° − θ.

The contact angle of hexadecane in water also depended on the hydrophilicity of the brushes. A hexadecane drop spread on the PFA-C_8 brush surface in water, whereas oleophobicity was observed by the contact angle measurement of hexadecane in air on the PFA-C_8 brush surface.[67] On the contrary, PMMA and PDHMA exhibited a higher contact angle of hexadecane in water in spite of the very low contact angle of hexadecane in air. The hexadecane droplet can easily spread on a hydrophilic surface in air because the surface free energies of hydrophilic brushes γ_{SV} are higher than that of hexadecane γ_{OV} (γ_{LV} = 27.6 mN/m in Table 1). In water, the contact angle of hexadecane is largely governed by γ_{SW} and γ_{OW}, where γ_{OW} is the interfacial energy at the hexadecane–water interface. As listed in Tables 1 and 5, γ_{OW} (γ_{LW} = 53.7 mN/m in Table 1) is significantly larger than γ_{SW} of the hydrophilic brushes to create a self-standing drop shape of hexadecane on the brush surface in water. Parameters γ_{SW}^{V} and γ_{SW}^{W} of the hydrophobic PFA-C_8 brush were 46.1 and 54.8 mN/m, respectively, which were close to the value of γ_{OW}. Therefore, a small contact angle of hexadecane in water was observed on the PFA-C_8 brush surface. Conversely, γ_{SW}^{W} of polar polymer brushes with hydrophilic functional groups were lower than γ_{SW}^{V}, indicating the reduction in the interfacial energy for the brush–water interface in the aqueous environment. The fully hydrated polymer brush in water formed a hydrophilic layer on the

dx.doi.org/10.1021/la301033h | Langmuir 2012, 28, 7212–7222

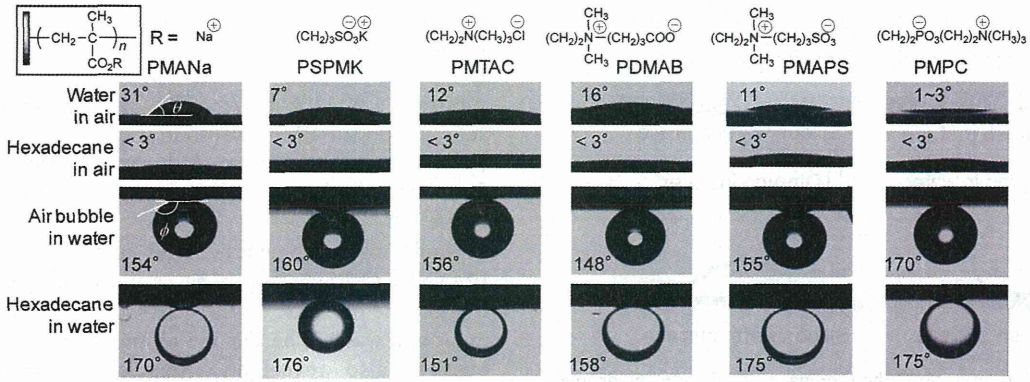

Figure 4. Photographs (side view) of water and hexadecane droplets on polyelectrolyte brushes in air and air bubbles and hexadecane droplets in contact with the brush surfaces in water.

substrate surface, which resulted in antifouling behavior against the hydrocarbon drops.

Surface Wettability of Ionic Polymer Brushes. A water droplet on the polyelectrolyte brush surface had a lower contact angle compared to those of droplets on nonionic-type hydrophilic polymer brushes, as shown in Table 4 and Figure 4. PMANa, PMTAC, PSPMK, PDMAB, and PMPC are water-soluble polymers, whereas PMAPS can be dissolved in an aqueous salt solution. Sulfobetaine groups in PMAPS strongly bind to each other by electrostatic interaction and do not disperse in deionized water at 298 K, resulting in a slightly higher contact angle (11°) for water than for the other zwitterionic-type polyelectrolyte brushes. Although the water contact angle of PMANa was relatively high (31°), the other polyanion, polycation, and zwitterionic-type polyelectrolyte brushes had smaller contact angles. In particular, a very small contact angle of water (3°) was observed on the PMPC brush surface because PMPC adsorbs moisture from the atmosphere like a deliquescent material does.

As shown in Table 5, the surface free energies of polyelectrolyte brushes evaluated by Owens' method were 70–74 mN/m, which were much higher than those of nonionic hydrophilic polymer brushes such as PMMA, PDHMA, and PVA brushes. The surface free energies of the polyelectrolyte brushes were also estimated by the three-liquid acid–base method proposed by van Oss, Chaudhury, and Good (vOCG)[25] in this study. The calculation process of the vOCG method and the surface free energies of polymer brushes are described in the Supporting Information.

When we estimate the surface free energies of the hydrophilic polymer brushes, another important issue to be considered is the partial wetting or total wetting of the hydrophilic polymer brush surface with water. Hydrophilic polymer brushes with a high graft density collapse or shrink in air or in the vapor phase but become hydrated in water to form an extended conformation due to the osmotic pressure. Therefore, the work of hydration at the edge of the brush where the water meets the vapor phase might be considered for the study of the water contact angle of the brush. Cohen Stuart et al. have reported the wetting of PEO brushes.[60] They studied the effect of the bridging of the water/vapor interface by the grafted PEO layer on partial wetting. Théodoly et al. studied the wetting with water of the surface of polystyrene (PS) covered with a poly(acrylic acid) (PAA) brush.[10] They explained how the wetting behavior was governed by the free enthalpy of hydration of the polyelectrolyte monomer units and interfacial tension among PS, PAA, water, and air and the pressure in the brush at the triple contact line of PAA brush–water–vapor. Complete wetting with water can be expected on the surfaces of water-soluble polyelectrolyte brushes such as PMANa and PMPC but might require microscopic observation of the water drop edge as it spreads on the brush surface.

Air Bubble and Oil Detachment from the Polyelectrolyte Brush Surface in Water. Figure 4 displays photographs of air bubbles and hexadecane droplets in water on a series of polyelectrolyte brush surfaces. Most of the air bubbles in contact with the brush surfaces formed spherelike shapes, although some bubbles were deformed by the buoyancy effect. The surfaces of the polyelectrolyte brushes repelled both air bubbles and hexadecane droplets in water. It was difficult to pin an air bubble on the brush surface in water because the bubble was easily swept away by slight vibrations and water flow. When the air bubble in water is released from the lower position and touches the polyelectrolyte brush surface, the air bubble bounces several times. A movie of an air bubble bouncing on the PMPC brush surface in water is available in the Supporting Information. The contact angles of air bubbles and hexadecane in water were observed to remain constant for at least 15–20 min. These results demonstrate the superhydrophilic surfaces prepared with polyelectrolyte brushes.

In air, a hexadecane droplet wets and spreads on the surfaces of polyelectrolyte brushes. However, once the brush substrate was dipped into water, hexadecane detached from the brush surface. Hexadecane and typical hydrocarbon liquids have lower density (0.7–0.8 g/mL) than water. Therefore, they quickly flowed out of the substrate in water. In this work, antifouling behavior in water was observed using silicone oil (Shin-Etsu Chemical Co. KF-96–100CS), the density of which (0.965 g/mL at 293 K) is relatively close to that of water. Figure 5 showed the contact angle of silicone oil on the surface of the PMPC brush and an unmodified silicon wafer in air and in water. The silicone oil immediately spread on the surface of the PMPC brush and the unmodified silicon wafer in air. However, once the brush substrate was dipped into water, the silicone oil quickly formed a sphere that eventually flowed out of the brush surface. The three-phase contact angle θ at the substrate/oil/water interface was 173°. By contrast, the silicone oil remained attached to the unmodified silicon substrate in water (θ = 56°). The movies of silicone oil detachment behavior on PMPC brush surface and nonmodified silicon wafer surface in water are available in the Supporting Information.

dx.doi.org/10.1021/la301033h | *Langmuir* 2012, 28, 7212–7222

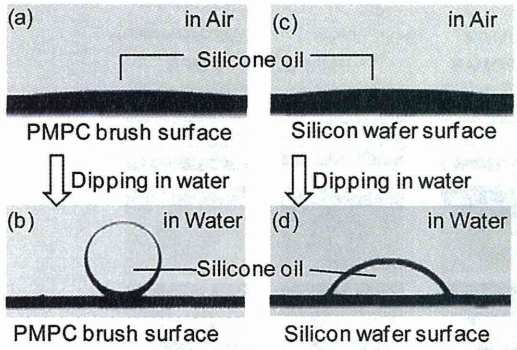

Figure 5. Wettability-reversion phenomena of a silicone oil droplet (5.0 μL, Shin-Etsu Chemical Co. KF-96-100CS) on a PMPC brush (a) in air and (b) in water and on an unmodified silicon wafer (c) in air and (d) in water. Photograph b (side view) displays an oil droplet on a PMPC brush substrate in water, showing the superoleophobicity, with a contact angle of 173°.

The work of adhesion is the amount of reversible work needed to separate a unit area of liquid from the substrate.[68] The work of adhesion in water[69,70] can be expressed as

$$W_{OWS} = \gamma_{SW} + \gamma_{OW} - \gamma_{SO} \quad (13)$$

Combining eqs 13 and 14 (Young's equation) provides a more useful expression for the work of adhesion, as given in eq 15

$$\gamma_{SW} - \gamma_{SO} = \gamma_{OW} \cos\theta \quad (14)$$

$$W_{OWS} = \gamma_{OW}(1 + \cos\theta) \quad (15)$$

Provided both γ_{OW} and θ can be measured experimentally, it is possible to calculate the work of adhesion of oil to the solid under water.[63]

The interfacial free energy (γ_{OW}) of silicone oil/water was estimated to be 7.2 mN/m by the sessile drop method combined with the Young–Laplace equation[71] and the curve-fitting calculation for the drop shape analysis using the density difference between the oil and water ($\Delta\rho$ = density of water (0.997) − density of oil (0.965) = 0.032 g/mL at 293 K). The γ_{OW} value of the silicone oil was much lower than the value of a typical hydrocarbon, such as hexadecane (53.3 mN/m), probably because of some additives in the dimethylsiloxane base oil or polar functional groups attached to the silicone molecules to improve the chemical stability of the product. Using eq 15, the W_{OWS} of silicone oil on the PMPC brush surface was 0.054 mN/m, and W_{ad} of the unmodified silicon substrate was 11.2 mN/m. The small value of the work of adhesion on the PMPC brush in water is assumed to be caused by the excellent affinity with water, which leads to the formation of a water-swollen brush layer and the beading up of the oil.

Similar oil detachment behavior in water was observed on the PMANa and PSPMK brushes, as shown in Figure 6. However, the silicone oil stuck on the PFA-C_8 and PMMA brushes both in air and water. The silicone oil on the PMTAC and PMAPS brushes also revealed a relatively high contact angle (approximately 160°) in water. However, the oil did not flow out from the substrates. In the case of the PMAPS brush, the contact angle of silicone oil increased with the addition of aqueous NaCl solution. When the concentration reached 1.0 M, the contact angle became almost 175°, as shown in Figure 6h, and the silicone oil eventually detached from the PMAPS brush. This oil detachment behavior is closely related to the hydration state of PMAPS. PMAPS is insoluble in deionized water at room temperature but soluble in aqueous salt solution.[72] The chain dimension of PMAPS in aqueous solution increased with the NaCl concentration, which was confirmed by light-scattering measurements and small-angle X-ray scattering.[73,74] Neutron reflectivity measurements revealed that the thickness of swollen PMAPS brushes in aqueous solution increased with the salt concentration from 0 to 1.0 M because the strong attractive dipole–dipole interaction among sulfobetaine units was moderated by the hydrated ions in the aqueous salt solution to induce the switching from a collapsed state to a well-hydrated brush state with a relatively extended chain structure.[75] As a result, the swollen PMAPS brush in aqueous NaCl solution effectively enhanced the oil repellence in aqueous solution. The antifouling effect on a polymer thin film bearing sulfobetaine units was also reported by Gleason.[76] Superhydrophilicity and water promoted the detachment behavior of air bubbles and oils.

The removal of oil drops from solid surfaces immersed in an aqueous medium is of interest in many applications such as self-cleaning, antifogging, and antifouling systems. Oleophobic and antifouling surfaces have been widely fabricated with conventional superhydrophobic materials such as fluoropolymers with micro/nanohierarchical structures like those in a lotus leaf. By

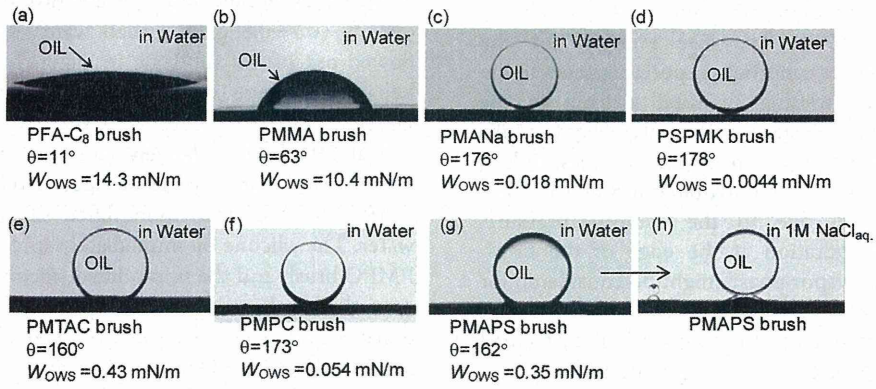

Figure 6. Photographs (side view) of a silicone oil droplet (5.0 μL, Shin-Etsu Chemical Co. KF-96-100CS) on (a) PFA-C_8, (b) PMMA, (c) PMANa, (d) PSPMK, (e) PMTAC, (f) PMPC, and (g) PMAPS brushes in water and (h) the PMAPS brush in a 1.0 M NaCl aqueous solution at 298 K. All of the substrates were immersed in water after the silicone oil was applied in air. The contact angle of the oil droplet in water and the work of adhesion are listed under the photographs.

dx.doi.org/10.1021/la301033h | Langmuir 2012, 28, 7212–7222